Pergamon

Int. J. Heat Mass Transfer. Vol. 40, No. 15, pp. 3627–3640, 1997

Printed in Great Britain
0017-9310/97 $17.00+0.00

PII: S0017-9310(96)00386-9

Fluid flow and heat transfer in a pipe with wall suction

D. SOFIALIDIS and P. PRINOS†
Department of Civil Engineering, University of Thessaloniki, Thessaloniki, Greece

(*Received* 16 *May* 1995 *and in final form* 28 *November* 1996)

Abstract—The effects of wall suction on turbulent fluid flow and heat transfer in a pipe were numerically studied using the Reynolds-averaged Navier–Stokes equations in conjunction with the temperature equation. Linear and non-linear k–ε or k–ω low-Re models of turbulence are used for 'closing' the governing equations. Computed mean velocity and temperature profiles were compared with analytical solutions and experimental measurements for suction rates between 0.46 and 2.53%. Analytical results, based on boundary layer assumptions and mixing length concepts, were found to be in satisfactory agreement with computed and experimental data for the lowest suction rate examined. However, for the highest rate, they did not follow the computed and experimental ones, especially in the near-wall region. Near-wall velocities and temperatures increased with increasing suction rate. Computed and experimental velocities and temperatures fell below the corresponding logarithmic law of the wall with no suction. Computed and experimental turbulent shear stress and heat flux were reduced by the presence of wall suction. The excess skin friction coefficient and Nusselt number, resulting from suction, were found to be up to 9 times the respective ones with no suction.© 1997 Elsevier Science Ltd.

INTRODUCTION

The study of wall suction effects on the flow characteristics and heat transfer rates in a pipe is of both practical and theoretical interest. Turbulent pipe flow with mass withdrawal from the wall (i.e. suction) is encountered in a variety of engineering applications, and it is well known that wall suction has a significant effect on mass, momentum and heat transfer rates. From a theoretical viewpoint wall suction, even at low rates, considerably affects the near-wall mean velocities and temperatures, and causes an alteration of the logarithmic law of the wall for the mean velocity and temperature. In addition, it increases the wall shear stress in the suction region, and reduces the turbulence levels and turbulent heat fluxes across the pipe radius.

Studies regarding the effects of wall suction on both flow characteristics and heat transfer rates are rather limited. Most of the studies deal with isothermal boundary layer or pipe flow with wall suction. The suction rate, defined as $A = V_w/U_{bo}$ (V_w = uniform suction velocity, U_{bo} = bulk inlet velocity), is usually small (up to 0.3%), for which a modified log law was found to be valid (Stevenson [1], Verollet *et al.* [2]).

Experimental studies on the wall suction effects in an isothermal pipe flow have been conducted by Weissberg and Berman [3], Aggarwal *et al.* [4] and Schildknecht *et al.* [5] among others.

Weissberg and Berman [3] experimentally studied the effect of uniform wall suction on the structure of fully developed pipe flow for suction rates up to 2%. They found that the suction effect reduced the longitudinal turbulence intensity across the whole pipe radius.

Aggarwal *et al.* [4] applied uniform wall suction rates up to $A = 2\%$ to a fully developed turbulent pipe flow for a length of 10 D (D is the pipe diameter). They measured the pressure drop, mean velocity profiles and turbulent intensities, and found that the latter, normalized with the local mean velocity, decreased in the central part of the pipe for low suction rates but increased for higher suction rates. However, the absolute levels of the turbulence intensities were found to decrease in both situations.

Brosh and Winograd [6] also presented experimental results for suction rates up to $A = 0.4\%$ applied for various pipe lengths (up to 40 D). They showed that a suction length above 40 D results in a decrease in turbulence levels as compared with those of pipe flow with no suction. They also suggested that mixing-length models may be inadequate to describe turbulent momentum transport in such flow conditions.

The most complete experimental study reported in the literature was performed by Schildknecht *et al.* [5]. Suction rates up to $A = 2.53\%$ were induced into a fully developed turbulent pipe flow using a 27 D long porous length. Detailed results of mean and turbulence characteristics along the suction region are given for a suction rate of $A = 0.46\%$, and are used in the present study for comparison purposes. Their results indicate that turbulent intensities are reduced by suction, as well as the maxima of the terms in the

† Author to whom correspondence should be addressed.

NOMENCLATURE

A	suction rate
C, C_θ	constants in the velocity and temperature law of the wall
c_f	skin friction coefficient
$c_{\varepsilon i}$, $c_{\varepsilon 2}$	constants of turbulence models
c_μ, $c_{\omega 1}$, $c_{\omega 2}$, f_ε, E	functions of turbulence models
c_I–c_{VII}	coefficients in the non-linear turbulent stress relation
D	pipe diameter
f_μ	damping function
K	momentum flux factor
l	turbulent mixing length
Nu	Nusselt number
P	mean static pressure
P_k	production of k due to shear
Pr, Pr_t	Prandtl number of fluid, and turbulent Prandtl number
q_w	wall heat flux
r	radial coordinate measured from pipe centreline
r_w	pipe radius
Re	Reynolds number based on the pipe diameter and bulk velocity
R_t	turbulent Reynolds number
S_{ij}	mean strain tensor
S	strain parameter
U, u	mean and fluctuating value of the axial velocity
U_*	friction velocity, $(\tau_w/\rho)^{1/2}$
$\overline{u^2}$, $\overline{v^2}$, $\overline{w^2}$, $\overline{uv}$	turbulent stresses
$\overline{u\theta}$, $\overline{v\theta}$	turbulent heat fluxes
V, v	mean and fluctuating value of the radial velocity
V_w	uniform wall suction velocity
x	axial coordinate
y	distance from the wall.

Greek symbols

β	eigenvalue
γ	transport parameter
Γ_θ	eddy diffusivity of heat
δ_{ij}	Kronecker delta
ε	dissipation rate of k
$\tilde{\varepsilon}$	isotropic dissipation rate of k
Θ, θ	mean and fluctuating value of temperature
Θ_*	friction temperature
κ, κ_θ	constants in the velocity and temperature law of the wall
ν, ν_t	kinematic viscosity of the fluid and eddy viscosity
σ_k, σ_ε, σ_ω	diffusion coefficients in the k, $\tilde{\varepsilon}$ and ω transport equations
τ_w	wall shear stress
Ω_{ij}	mean vorticity tensor
Ω	vorticity parameter.
ω	dissipation variable used in the k–ω model.

Subscripts

b	local bulk value
o	value upstream of the suction region
w	value at the wall.

Superscripts

+	value normalized by means of the friction velocity.

turbulent kinetic energy equation. In addition, more uniform axial mean velocity, U, distributions were measured due to suction as the near-wall layers are accelerated, and the core flow is decelerated by the increasing radial velocity component, V.

The effects of wall suction on both mean flow and heat transfer rates have been studied experimentally by very few investigators due to the complexity of the experimental set-up. Elena [7, 8] has experimentally studied the wall suction effects on a heated pipe flow for suction rates up to 0.3%. He measured mean velocities and temperatures as well as turbulent characteristics (intensities, shear stress, heat flux), and found that the above characteristics are reduced with increasing suction rate.

Verollet *et al.* [2] have conducted a similar experimental study in a heated boundary layer with wall suction rates up to 0.3%. They found that the modified law of the wall with suction, proposed by Stevenson [1], fits the experimental measurements, and proposed an analogous thermal law of the wall for the mean temperatures.

Antonia *et al.* [9] have also examined the effect of wall suction on the organized motion of a slightly heated turbulent boundary layer. They measured a reduction in the Reynolds shear stress and lateral turbulent heat flux, although the skin-friction coefficient and Stanton number increase due to the additional momentum and thermal fluxes associated with the suction velocity.

Analytical studies have been performed by Kinney and Sparrow [10] and Merkine *et al.* [11] for non-isothermal pipe flow with wall suction, and also by Medeiros *et al.* [12] and Silva-Freire [13] for a non-isothermal turbulent boundary layer with low suction rates.

Kinney and Sparrow [10] developed a turbulent transport model, based on the mixing-length concept, to calculate the mean streamwise velocity and temperature profiles, as well as heat and mass transfer

rates, in turbulent pipe flow with wall suction rates up to $A = 2\%$. Their model was based on a modified van Driest [14] damping function appropriate for wall suction and the final integrodifferential equation for U^+ ($U^+ \equiv U/U*$, where U = local mean axial velocity, and $U*$ = friction velocity) was solved iteratively. Friction factor, pressure drop, heat and mass transfer coefficients were calculated for various suction rates from $A = 0$–2%, and were found to be affected considerably even for very low suction rates. Predictions by the model were compared against the experimental measurements of Weissberg and Berman [3] for suction rates up to $A = 0.5\%$.

Merkine *et al.* [11] used the same model with the previous investigators, but they applied a modified damping function. They claimed that their model yielded better results than those of Kinney and Sparrow [10], especially when the pressure drop was compared with the experimental measurements of Weissberg and Berman [3].

Medeiros *et al.* [12] have proposed expressions which give a detailed account of the temperature distributions in the inner and outer regions of an incompressible boundary layer. An equation for the Stanton number has also been proposed which gives good predictions.

Numerical studies of the suction effects on turbulent pipe flow are rather scarce. To the author's knowledge, the only study is that of So and Yoo [15], who tested a low-*Re* stress model of turbulence as well as a low-*Re* k–ε turbulence model, against the experimental data of Weissberg and Berman [3]. The latter model overpredicted the axial pressure drop and underestimated the mean velocity in the region away from the wall. Near-wall predictions of mean velocity were similar in both models: however, the former model did not predict the peak of turbulence intensity near the wall for all suction rates examined.

In the present work, the wall suction effects on pipe flow and heat transfer are studied numerically using the Reynolds-averaged Navier–Stokes equations and the temperature equation in conjunction with k–ε and k–ω eddy viscosity models (EVMs) of turbulence of the low-*Re* type. Models of this kind are capable of describing all flow features up to the wall, which is necessary for such flow conditions since conventional wall functions are known to be inadequate for flows with wall mass transfer.

The k–ε models used are those of Launder and Sharma [16] and Craft *et al.* [17] slightly modified according to Suga [18], while the k–ω models employed are those of Wilcox [19] and Sofialidis [20]. These models are called for brevity LS, CLS, W93 and SOF, respectively, in subsequent paragraphs. The CLS and SOF EVMs differ from the conventional low-*Re* ones in two aspects. First, they employ a nonlinear constitutive relation with strain and vorticity invariant dependency for the description of the Reynolds stresses. Second, to simulate the turbulence damping that occurs near solid boundaries they do not only use empirical damping functions, f_μ, but they also introduce damping caused by the strain rate of the flow.

Computational results are compared against detailed experimental measurements performed by Schildknecht *et al.* [5] for isothermal conditions. In addition, computed normalized temperatures and heat transfer characteristics are compared against the non-isothermal measurements of Elena [7, 8] for similar flow and thermal conditions. Numerical and experimental results are compared with analytical solutions, based on the model of Kinney and Sparrow [10] and the improved version of Merkine *et al.* [11], and the limitations and inadequacies of the analytical models are highlighted.

The effects of wall suction on the mean and turbulence characteristics are examined at two stations ($x/D = 1.358$ and 2.213) inside the suction region where the flow is found to be in a 'fully developed' state and experimental measurements are available for two suction rates ($A = 0.46$ and 2.53%). The comparison entails profiles of the mean streamwise velocity, mean temperature, turbulent shear stress and heat flux along the pipe radius. Finally, attention is given to the variation of the skin friction coefficient and the Nusselt number along the suction region.

2. GOVERNING EQUATIONS AND THEORETICAL CONSIDERATIONS

The equations governing the steady, incompressible, two-dimensional turbulent pipe flow with heat transfer are the Reynolds-averaged Navier–Stokes equations and the temperature equation which can be written in cylindrical coordinates as follows:

continuity equation

$$\frac{\partial}{\partial x}(rU)+\frac{\partial}{\partial r}(rV)=0 \tag{1}$$

x-*momentum equation*

$$\frac{\partial}{\partial x}(rU^2)+\frac{\partial}{\partial r}(rVU) = -r\frac{\partial P}{\partial x}+r\frac{\partial}{\partial x}\left[\nu\left(\frac{\partial U}{\partial x}+\frac{\partial U}{\partial x}\right)-\overline{u^2}\right] + \frac{\partial}{\partial r}\left\{r\left[\nu\left(\frac{\partial U}{\partial r}+\frac{\partial V}{\partial x}\right)-\overline{uv}\right]\right\} \tag{2}$$

r-*momentum equation*

$$\frac{\partial}{\partial x}(rUV)+\frac{\partial}{\partial r}(rV^2) = -r\frac{\partial P}{\partial r} + r\frac{\partial}{\partial x}\left[\nu\left(\frac{\partial V}{\partial x}+\frac{\partial U}{\partial r}\right)-\overline{uv}\right]$$

$$+\frac{\partial}{\partial r}\left\{r\left[v\left(\frac{\partial V}{\partial r}+\frac{\partial V}{\partial r}\right)-\overline{v^2}\right]\right\}-\frac{2vV}{r}-\overline{w^2} \quad (3)$$

temperature equation

$$\frac{\partial}{\partial x}(rU\Theta)+\frac{\partial}{\partial r}(rV\Theta)=r\frac{\partial}{\partial x}\left(\frac{v}{Pr}\frac{\partial\Theta}{\partial x}-\overline{u\theta}\right)+\frac{\partial}{\partial r}\left[r\left(\frac{v}{Pr}\frac{\partial\Theta}{\partial r}-\overline{v\theta}\right)\right] \quad (4)$$

where x and r = axial and radial coordinates, respectively, U and V = corresponding mean velocity components, Θ = mean temperature, P = mean pressure, v = kinematic viscosity of the fluid, Pr = Prandtl number of the fluid (0.71 for air), $\overline{u^2}$, $\overline{v^2}$, $\overline{w^2}$ and $\overline{uv}$ = turbulent stresses, and $\overline{u\theta}$ and $\overline{v\theta}$ = turbulent heat fluxes.

Kinney and Sparrow [10] ignored the streamwise diffusion terms of equations (2) and (4), and postulated that locally self-similar profiles exist for the velocity and temperature in the case of uniform suction:

$$\frac{U}{U_b}=f\left(\frac{r}{r_w}\right)\quad\frac{\Theta-\Theta_w}{\Theta_b-\Theta_w}=g\left(\frac{r}{r_w}\right) \quad (5)$$

where U_b = bulk velocity, Θ_w = wall temperature, Θ_b = bulk temperature, and r_w = pipe radius.

Hence, the x-momentum and temperature equations are transformed to a non-linear integrodifferential equation for the non-dimensional velocity U^+, and to a differential equation for the function g, respectively. These equations are written in the following form:

$$\frac{dU^+}{dy^+}+(l^+)^2\left(\frac{dU^+}{dy^+}\right)^2=\frac{r^+}{r_w^+}-\left(\frac{V_w}{U_b}\right)\times\left[\frac{Re}{2}-\frac{2}{r_w^+}\int_0^{y^+}U^+(r_w^+-y^+)dy^+\right]\frac{U^+}{r^+}+4\left(\frac{V_w}{U_b}\right)\frac{1}{r_w^+}\left\{\left[1-\left(\frac{r^+}{r_w^+}\right)^2\right]\frac{Re^2}{8}K-\int_0^{y^+}(U^+)^2(r_w^+-y^+)dy^+\right\}\frac{1}{r^+} \quad (6)$$

$$\frac{d}{dy^+}\left[(r_w^+-y^+)\gamma\frac{dg}{dy^+}\right]+(r_w^+-y^+)V^+\frac{dg}{dy^+}+(r_w^+-y^+)U^+g\frac{\beta^2}{r_w^+\,Re\,Pr}=0 \quad (7)$$

where y^+ = normalized distance from the wall ($yU*/v$), 1^+ = normalized turbulent mixing length ($lU*/v$), r^+ = normalized radial distance ($rU*/v$), Re = bulk Reynolds number, K = momentum flux factor, γ = transport parameter $(1/Pr)+(l^+)^2dU^+/dy^+]$, and β = eigenvalue.

Equation (6) contains four parameters, V_w/U_b, Re, r_w^+ and K, and is solved iteratively with given values of V_w/U_b and Re, and a boundary condition of $U^+=0$ at $y^+=0$. The mixing length l^+ is described with an appropriate relationship which takes into account the effect of suction [10, 11]. Equation (7) is solved in conjunction with the boundary conditions $g=0$ at $y^+=0$ and $dg/dy^+=0$ at $y^+=r_w^+$, with the distributions of U^+ and V^+ known from equations (6) and (1), while the parameters Re and Pr are prescribed.

Stevenson [1] and Verollet *et al.* [2] further simplified equations (2) and (4), assuming boundary layer conditions with zero pressure gradient and streamwise gradients much lower than the vertical ones ($\partial/\partial x \ll \partial/\partial y$).

Based on the above assumptions and applying the mixing-length concept, the following modified logarithmic laws for both velocity and temperature are derived:

$$\frac{2}{A^+}\left[1-(1-A^+U^+)^{1/2}\right]=\frac{1}{\kappa}\ln y^+ + C \quad (8)$$

$$\frac{2Pr_t}{A^+}\left[1-(1-A^+\Theta^+)^{1/2Pr_t}\right]=\frac{1}{\kappa_\theta}\ln y^+ + C_\theta \quad (9)$$

where $A^+=V_w/U*$, Θ^+ = non-dimensional temperature $[(\Theta_b-\Theta)/\Theta*$, $\Theta*$ = friction temperature], κ = von Karman constant (= 0.42), $\kappa_\theta=\kappa/Pr_t$ (Pr_t = turbulent Prandtl number equal to 0.9) and C and C_θ = constants (5.5 and 3.2, respectively).

The above analysis is expected to hold for low suction rates where the boundary layer assumptions are valid. In case that the streamwise gradients are significant, all the terms in the x-momentum equation should be included, and the above analysis may lead to significant errors.

In the present study, equations (1)–(4) are solved numerically with all terms included in the calculation (elliptic problem) without making any assumptions. In addition, the calculation of the shear stress is not based on the mixing-length concept: instead, the eddy visocity, v_t is estimated through the calculation of the turbulent kinetic energy, k, and a second variable that is related to its dissipation rate, ε. The models of turbulence employed are two-equation EVMs, using transport equations for k and $\tilde{\varepsilon}$ or ω. Their exact formulation and features are described in the next section.

3. TURBULENCE MODELS

3.1. *The eddy viscosity/diffusivity concept, linear and non-linear formulations*

It is well known that the governing equations (1)–(4) contain additional unknowns, the Reynolds stresses and the turbulent heat fluxes, which have to

Table 1. Constants of the non-linear Reynolds stress expression

Model	c_{I}	c_{II}	c_{III}	c_{IV}	c_{V}	c_{VI}	c_{VII}
CLS	−0.1	0.1	0.26	$-10c_\mu$	0	$-5c_\mu$	$5c_\mu$
SOF	−0.08	0.08	0.18	−1.0	0	−0.1	0.1

be prescribed in order to arrive at a 'closed' system of equations. In the present investigation, the turbulence models serving this purpose, are of the 'eddy viscosity/diffusivity' type, and they employ two transport equations, one for the turbulent kinetic energy, k and a second for a variable related to ε, the dissipation rate of k.

The description of the turbulent stresses and heat fluxes is made through the eddy viscosity/diffusivity concept, which links them with the eddy viscosity, ν_t, and the eddy diffusivity of heat, Γ_θ, as follows:

$$\overline{u_i u_j} = -\nu_t S_{ij} + \frac{2}{3}\delta_{ij}k \quad \overline{u_i\theta} = -\Gamma_\theta \frac{\partial \Theta}{\partial x_i} \tag{10}$$

where S_{ij} = mean strain tensor $(\partial U_i/\partial x_j + \partial U_j/\partial x_i)$, δ_{ij} = Kronecker delta, and Γ_θ = eddy diffusivity of heat (ν_t/Pr_t).

The linear models of this study (LS k–ε model and W93 k–ω model) use equation (10) for the turbulent stresses, while the other two models (CLS k–ε and SOF k–ω) use the same relation with additional non-linear terms, namely quadratic and cubic terms of the strain, S_{ij}, and vorticity tensor, $\Omega_{ij}(\partial U_i/\partial x_j - \partial U_j/\partial x_i)$ as proposed by Craft *et al.* [17]:

$$\begin{aligned}\overline{u_i u_j} = &-\nu_t S_{ij} + \frac{2}{3}\delta_{ij}k + c_{\mathrm{I}}\nu_t\frac{k}{\varepsilon}\left(S_{ik}S_{kj} - \frac{1}{3}S_{kl}S_{kl}\delta_{ij}\right)\\ &+ c_{\mathrm{II}}\nu_t\frac{k}{\varepsilon}(\Omega_{ik}S_{kj} + \Omega_{jk}S_{ki}) + c_{\mathrm{III}}\nu_t\frac{k}{\varepsilon}\left(\Omega_{ik}\Omega_{jk} - \frac{1}{3}\Omega_{lk}\Omega_{lk}\delta_{ij}\right)\\ &+ c_{\mathrm{IV}}c_\mu\nu_t\frac{k^2}{\varepsilon^2}\left(S_{kl}\Omega_{ij} + S_{kj}\Omega_{li} + \frac{2}{3}S_{km}\Omega_{lm}\delta_{ij}\right)S_{kl}\\ &+ c_{\mathrm{V}}c_\mu\nu_t\frac{k^2}{\varepsilon^2}\left(S_{ik}S_{jl} - \frac{1}{3}S_{mk}S_{ml}\delta_{ij}\right)S_{kl}\\ &+ c_{\mathrm{VI}}c_\mu\nu_t\frac{k^2}{\varepsilon^2}S_{ij}S_{kl}S_{kl} + c_{\mathrm{VII}}c_\mu\nu_t\frac{k^2}{\varepsilon^2}S_{ij}\Omega_{kl}\Omega_{kl}.\end{aligned} \tag{11}$$

It should be pointed out that, when the SOF k-ω model is used, the ratio k/ε, appearing in equation (11), is replaced by definition with $1/\omega$. The values of the constants in the above equation are given in Table 1.

The eddy viscosity, appearing in equations (10) and (11) is expressed as a function of the two independent variables, k and $\tilde{\varepsilon}$ [isotropic dissipation rate of k: $\tilde{\varepsilon} \equiv \varepsilon - 2\nu(\partial\sqrt{k}/\partial x_j)^2$ or ω for the k–ε and k–ω models, respectively]. It is expressed as $\nu_t = c_\mu f_\mu k^2/\varepsilon$ or $\nu_t = c_\mu f_\mu k/\omega$, where c_μ and f_μ are constants or functions. Conventional low-*Re* models use damping functions, f_μ for the approximation of the near-wall turbulence damping which are related to a viscosity-dependent parameter, the local turbulent Reynolds number, $R_t(k^2/\nu\varepsilon$ or $k/\nu\omega)$. Models of this type are the LS k–ε and W93 k–ω models used in the present investigation. On the other hand, the CLS k–ε and SOF k–ω models use strain, S $[k(0.5S_{ij}S_{ij})^{0.5}/\varepsilon]$, and vorticity, $\Omega[k(0.5\Omega_{ij}\Omega_{ij})^{0.5}/\varepsilon]$ parameters to simulate the turbulence damping, allowing c_μ to vary with max $[S,\Omega]$. Nevertheless, this is not sufficient to introduce the necessary damping effect, and damping is supplemented by the use of damping functions, f_μ. The constants or functions c_μ and f_μ of the various models used are given in Table 2.

3.2. k *and* $\tilde{\varepsilon}$ *or* ω *transport equations*

The task of 'closing' the system of equations entails two transport equations for two turbulent variables. The modelled equation for the turbulent kinetic energy, k, has the following form, in cylindrical coordinates, for all the models employed in this study:

k *equation*

$$\begin{aligned}\frac{\partial}{\partial x}(rUk) + \frac{\partial}{\partial r}(rVk) = &\, r\frac{\partial}{\partial x}\left[\left(\nu + \frac{\nu_t}{\sigma_k}\right)\frac{\partial k}{\partial x}\right]\\ &+ \frac{\partial}{\partial r}\left[r\left(\nu + \frac{\nu_t}{\sigma_k}\right)\frac{\partial k}{\partial r}\right] + r(P_k - \varepsilon)\end{aligned} \tag{12}$$

where P_k = production of k due to shear $(\overline{-u_i u_j}\partial U_i/\partial x_j)$, and σ_k = model constant (1.0 for both LS and CLS models, 2.0 for the W93 model, and 1.2 for the SOF model). The production term, P_k, is evaluated through equations (10) or (11) depending on the choice of the model.

The second transport equation used is that for $\tilde{\varepsilon}$, when the LS and CLS models are employed. $\tilde{\varepsilon}$ and ε take quite different values near solid boundaries, and tend to coincide away from them. An ω-equation is used in the W93 and SOF models. The relation between ε (and equivalently $\tilde{\varepsilon}$) and ω is simply $\omega = \varepsilon/k = \tilde{\varepsilon}/k$. The corresponding equations are shown below:

$\tilde{\varepsilon}$*-equation*

$$\begin{aligned}\frac{\partial}{\partial x}(rU\tilde{\varepsilon}) + \frac{\partial}{\partial r}(rV\tilde{\varepsilon}) = &\, r\frac{\partial}{\partial x}\left[\left(\nu + \frac{\nu_t}{\sigma_\varepsilon}\right)\frac{\partial \tilde{\varepsilon}}{\partial x}\right]\\ &+ \frac{\partial}{\partial r}\left[r\left(\nu + \frac{\nu_t}{\sigma_\varepsilon}\right)\frac{\partial \tilde{\varepsilon}}{\partial r}\right] + r\left(c_{\varepsilon 1}\frac{\tilde{\varepsilon}}{k}P_k - c_{\varepsilon 2}f_\varepsilon\frac{\tilde{\varepsilon}^2}{k}\right) + E\end{aligned} \tag{13}$$

ω*-equation*

Table 2. c_μ and f_μ constants/functions appearing in the eddy viscosity relation†

Model	f_μ	c_μ
LS	$\exp[-3.4/(1+R_t/50)^2]$	0.09
CLS	$1-0.9\exp[-(R_t/30)^2]$	$\frac{0.3}{1+0.35S'^{1.5}}\left\{1-\exp\left[-\frac{0.36}{\exp[0.75S']}\right]\right\}$
W93	$\frac{0.025-(R_t/6.0)}{1.0+(R_t/6.0)}$	$0.09\frac{(5.0/18.0)+(R_t/8.0)^4}{1.0+(R_t/8.0)^4}$
SOF	$1-0.72\exp(-0.0056R_t)$	$0.09\left(\frac{3.89}{S'}-0.089\right)(1-\exp[-0.3S'-0.15S'^2])$

† $S' \equiv \max(S, \Omega)$.

Table 3. Model constants/functions appearing in the $\tilde{\varepsilon}$ and ω transport equations

k–ε	f_ε	E
LS	$1-0.3\exp(-R_t^2)$	$2\nu\nu_t\left(\frac{\partial^2 U_i}{\partial x_k \partial x_l}\right)^2$
CLS	$1-0.3\exp(-R_t^2)$	$2\nu\nu_t\left(\frac{\partial^2 U_i}{\partial x_k \partial x_l}\right)^2, \quad R_t > 100$
		$0.0095S\frac{k^2}{\tilde{\varepsilon}}\nu_t\left(\frac{\partial^2 U_i}{\partial x_k \partial x_i}\right)^2, \quad R_t < 100$
k–ω	$c_{\omega 1}$	$c_{\omega 2}$
W93	$\frac{5}{9}\frac{0.1+(R_t/2.7)}{1.0+(R_t/2.7)}\frac{1}{f_\mu}$	3/40
SOF	$0.435+2.17[\exp(-0.3R_t)]$	$0.833+2.17[\exp(-R_t/3.0)]$

$$\frac{\partial}{\partial x}(rU\omega)+\frac{\partial}{\partial r}(rV\omega)=r\frac{\partial}{\partial x}\left[\left(\nu+\frac{\nu_t}{\sigma_\omega}\right)\frac{\partial\omega}{\partial x}\right]+\frac{\partial}{\partial r}\left[r\left(\nu+\frac{\nu_t}{\sigma_\omega}\right)\frac{\partial\omega}{\partial r}\right]+r\left(c_{\omega 1}\frac{\omega}{k}P_k-c_{\omega 2}\omega^2\right) \quad (14)$$

where σ_ε, $c_{\varepsilon 1}$ and $c_{\varepsilon 2}$ = constants of the LS and CLS models (1.3, 1.44 and 1.92 for both models) σ_ω = constant of the k–ω models (2.0 for the W93 model, and 0.8 for the SOF model), and $c_{\omega 1}$, $c_{\omega 2}$, f_ε and E = model functions (Table 3).

4. NUMERICAL METHOD AND BOUNDARY CONDITIONS

The governing equations (1)–(4), (12) and (13) or (14) were solved by a finite volume method for elliptic flows (Huang and Leschziner [21]) in a computational domain shown in Fig. 1. The main characteristics of the numerical method are:

(a) The QUICK scheme is used for the discretization of the advection terms.
(b) The PISO method is applied for the pressure correction.
(c) The TDMA algorithm is used for solving the algebraic equations resulting after the discretization of the partial differential equations.

With regard to Fig. 1 the following boundary conditions are imposed:

(a) INLET: at the domain inlet fully developed profiles of U, Θ, k and $\tilde{\varepsilon}$ or ω were prescribed taken from previous parabolic computations, while the radial velocity component, V, was set to zero. The PASSABLE parabolic code was used (Leschziner

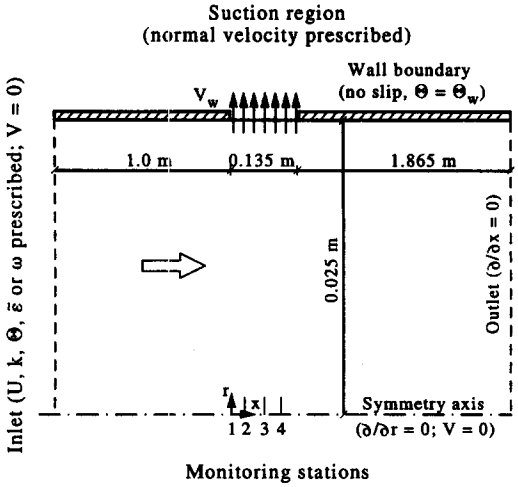

Fig. 1. Flow geometry and boundary conditions.

[22]), employing the same models as those used in the subsequent elliptic computations. These profiles resulted from computations with a given axial pressure gradient (dp/dx) corresponding to the upstream friction velocity of the experiment, $U_{*o} = 0.29$ ms^{-1}. With no suction, the solutions for most of the models resulted in slightly different inlet Reynolds number, Re_{bo}, than that observed in the experiments (maximum error + 1%). The W93 model only underestimated the bulk velocity and the respective Reynolds numbers by 7.8%. In addition, computed and experimental results were found to satisfactorily reproduce the law of the wall with no suction. This comprised a check for the performance of the various models used in well-known flow conditions.

(b) SYMMETRY AXIS: all gradients with respect to the radial direction, $\partial/\partial r$, were set equal to zero and the radial velocity component, V, was also set to zero.

(c) OUTLET: all gradients with respect to the axial direction, $\partial/\partial x$ were set to zero, corresponding to the assumption for fully developed flow. The length from the suction outlet to the domain outlet was proven to be long enough to allow a fully developed state to be reached again (i.e. uniform streamwise pressure gradient along the radius). This was essential for convenient boundary conditions to be imposed at the domain outlet, and preliminary runs confirmed that the fully developed state was actually reached. The V-velocity component was not set to zero but it was obtained from local continuity. However, the U-velocity profile was corrected to satisfy the overall continuity, taking into account the abstracted flow.

(d) WALL: the no-slip condition was employed for the velocities ($U = V = 0$) except along the suction region, where the V-velocity was given a constant value corresponding to the uniform suction rate under investigation. In addition, the temperature was given on the pipe wall, and k and $\tilde{\varepsilon}$ were set to zero. However, when the k–ω models are used, ω is calculated at the first node adjacent to the wall by the relationship $\omega = 6\nu/c_{\omega 2}y^2$ (y = distance from the wall) as proposed by Wilcox [19]. The condition is derived from the requirement that, in the ω-equation, molecular diffusion balances dissipation in the viscous sublayer. That was an additional reason for the grid to be sufficiently fine to resolve the near-wall region.

5. ANALYSIS OF RESULTS

Initially a grid-independence study was performed for checking the effect of grid refinement on the computed results. An orthogonal, non-uniform grid of 190×128, in the axial and radial direction, respectively, was employed initially. The grid was fine at the suction inlet and outlet planes. It employed 51 nodes upstream of the suction region (33.3% of the computational length), 116 nodes covered the suction region (4.5%), and, finally, 23 nodes were used downstream up to the domain outlet (62.2%).

Computations with all the models and for suction rates up to $A = 3\%$ proved that at least 30 grid nodes were located inside the viscous sublayer (y^+2), and therefore the assumptions involved in the low-Re models were satisfied.

With the above grid arrangement, the results are considered to be grid-independent since subsequent calculations with doubling of the grid did not produce considerable changes. For the sake of brevity, no results are presented from the grid independence tests.

The effects of wall suction on the mean velocity and temperature distribution are examined at two stations ($x/D = 1.358$ and 2.213) where the flow is in a 'fully developed' state. Computed velocities are compared against the experimental measurements of Schildknecht *et al.* [5] for two suction rates A (0.46 and 2.53%).

Figure 2(a) and (b) shows the experimental and computed axial velocity distribution at the above-mentioned stations for the lowest suction rate ($A = 0.46\%$). The measured velocities without suction are also included, and hence the effects of wall suction on the velocity distribution are clearly shown. The wall suction effect is to increase the near-wall velocities, and to reduce the respective ones near the centreline. The velocity profile has become more uniform, and the near-wall velocities are slightly higher than those with no suction due to the low suction rate. The wall layers are accelerated, and the central flow is decelerated due to the increasing radial velocity component. The computed velocity distributions by the various models are similar, and have the same features observed in the experiments. The results computed by the W93 model are shown to be closer to the measurements, especially in the near-wall

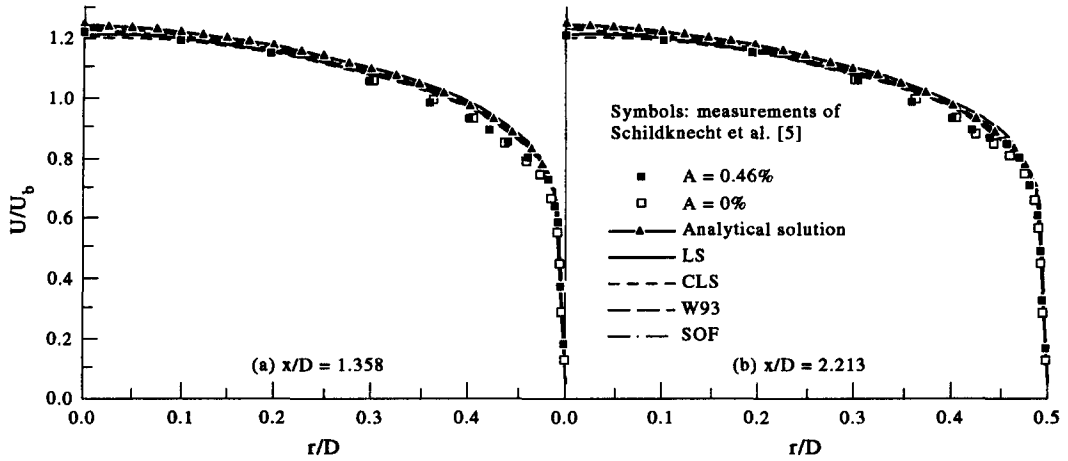

Fig. 2. Experimental, analytical and computed axial velocity distribution for $A = 0.46\%$.

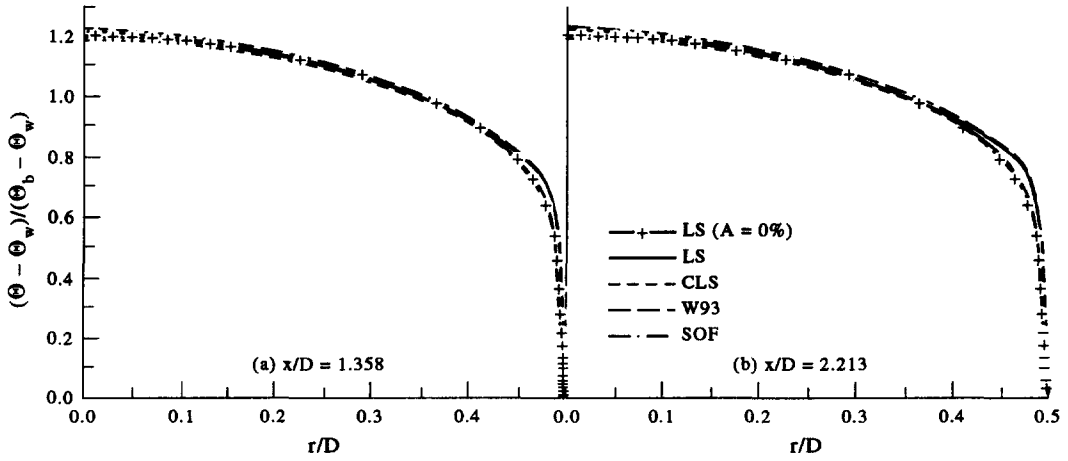

Fig. 3. Computed temperature distribution for $A = 0.46\%$.

region. In Fig. 2, the analytical solution, after solving equation (6) with a method similar to that presented by Kinney and Sparrow [10], is compared with experimental and computed results. Analytical results are in satisfactory agreement with computed and experimental data, indicating that the assumptions involved in the analysis are valid for such a low suction rate.

The wall suction effects on the temperature distribution are similar to those for the velocity distribution [Fig. 3(a) and (b)]. Mean normalized temperatures increased in the near-wall region, and decreased in the core region. The shape of the temperature profile is similar to that of the velocity in both stations.

The above-mentioned wall suction effects are more pronounced for the higher suction rate (2.53%), as Figs. 4 and 5 indicate. Both velocity and temperature profiles become quite flat, when compared with the respective profiles with no suction, with increased velocities and normalized temperatures near the pipe wall. All models well reproduce the effects of such a high suction rate on the velocity distribution with a slight overestimation of the velocities in the near-wall region at $x/D = 2.213$, and a corresponding underestimation in the central region. By comparing Figs 4 and 5, it is seen that a similarity between the velocity and temperature profiles is also valid with such a strong suction rate. Analytical results underestimate the near-wall velocities, providing a smooth velocity profile. For such a high suction rate, streamwise diffusion, which is ignored in the analytical solution, may be important, and may be the cause of the discrepancy between analytical and experimental or computed results in the near-wall region.

Figure 6(a) and (b) shows computed velocity for all models against y^+ for the two suction rates examined, together with those for no suction. In addition, the law for the wall with no suction is included, indicating the good performance of all the turbulence models used in fully developed pipe flow. It is shown that computational results fall below the logarithmic law with no suction. Such a fall increases with increasing suction rate. The laminar sublayer is shown to decrease with increasing wall suction. Computed vel-

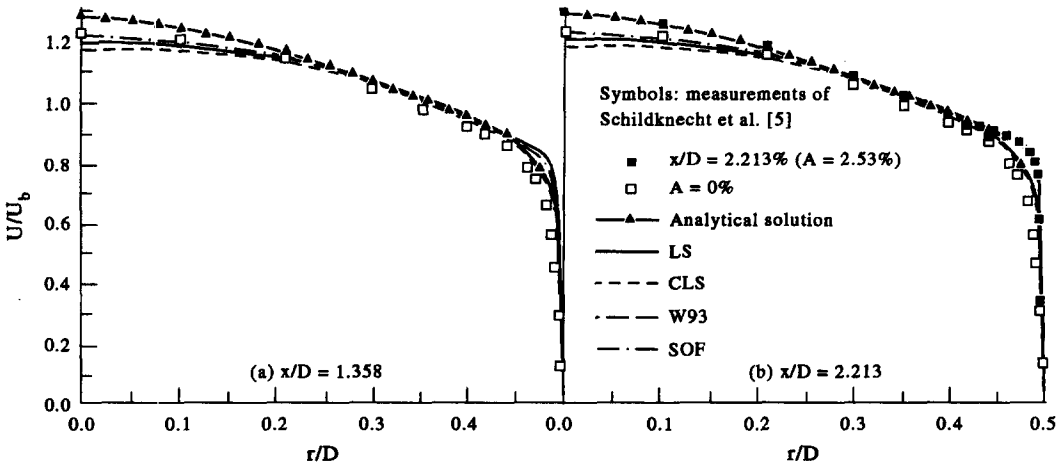

Fig. 4. Experimental, analytical and computed axial velocity distribution for $A = 2.53\%$.

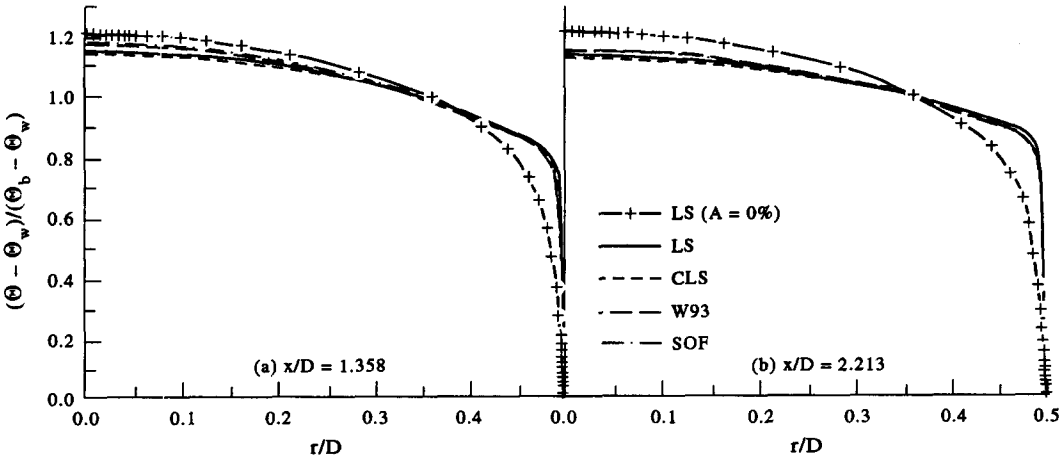

Fig. 5. Computed temperature distribution for $A = 2.53\%$.

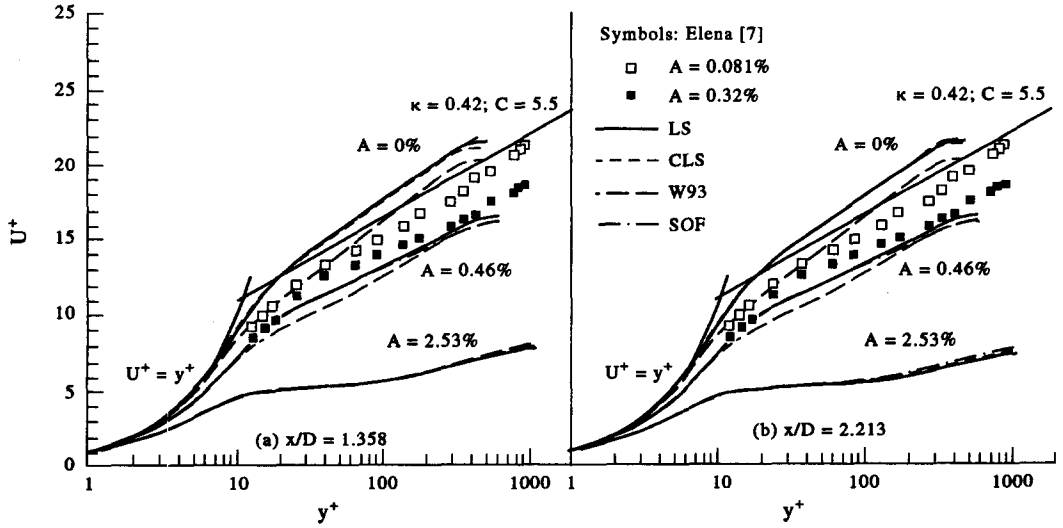

Fig. 6. Experimental and computed axial velocity profiles in wall coordinates.

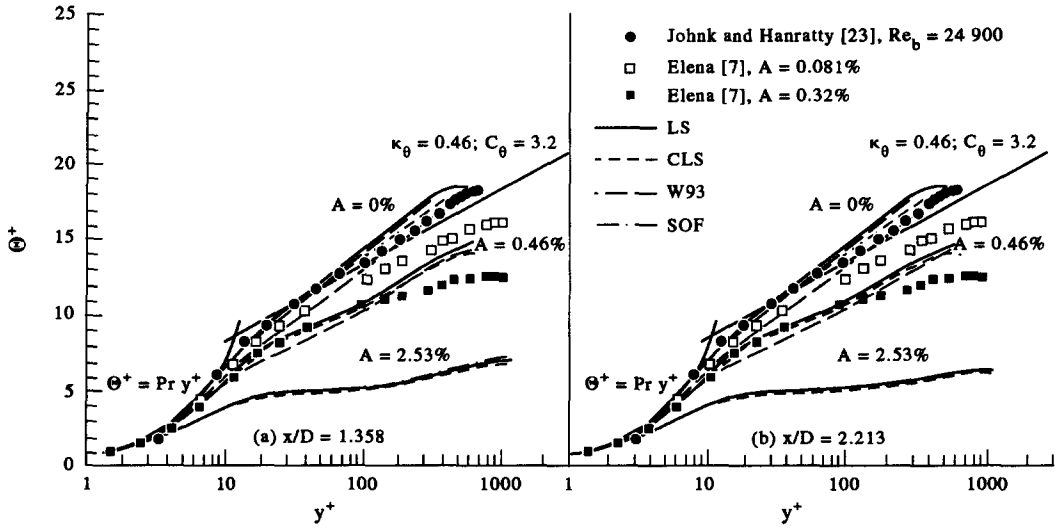

Fig. 7. Experimental and computed temperature profiles in wall coordinates.

ocities are shown to deviate from the law of the viscous sublayer for y^+ greater than 2. The slope of the profile in the logarithmic region for $A = 0.46\%$ is shown to be the same as the one with no suction, indicating that the von Karman constant κ of the law for the wall remains constant for low suction rates.

However, for the highest suction rate the slope of the curve changes as well as the constant C. In Fig. 6, the experimental results of Elena [7] are included for two low suction rates ($A = 0.081$ and 0.32%) which fall between the computed results for $A = 0$ and 0.46%, indicating that the shear velocity $U*$ is calculated correctly by all of the models, and, hence, the fall of the velocity profile below the log law of the wall is correctly predicted.

Similar phenomena are observed for the temperature profiles in wall coordinates [Fig. 7(a) and (b)]. Computed profiles fall below the thermal law for the wall with no suction, while the experimental results of Elena [7] for $A = 0.081$ and 0.32% fall between the computed curves for $A = 0$ and 0.46%, indicating the adequacy of the turbulent models in predicting temperature profiles for such flow conditions. In addition, computed results for no suction are compared satisfactorily with the measurements of Johnk and Hanratty [23] for similar Re. The temperature measurements for $A = 0.32\%$ start to deviate from the computed values for y^+ greater than 200, but this may be due to the different Re used in the experiments and computations.

The wall suction effects on the turbulent shear stress uv are shown in Fig. 8(a) and (b) for $A = 0.46\%$. A reduction in the absolute levels in the suction region is observed in both experimental and computed results, which indicates that even small suction rates tend to destroy turbulence and inverse transition to laminar flow is expected to occur for a long suction region. The propagation of the suction effects from the wall to the interior of the flow is well computed by all models, with those of LS and SOF performing better than the other models. The above reduction in the turbulent shear stress is more exaggerated when they are normalized with the local shear velocity $U*$, which is increased in the suction region.

A similar reduction in the normal turbulent heat flux $v\theta$ is observed for $A = 0.46\%$ at the two stations [Fig. 9(a) and (b)]. Computed results of $v\theta$ for no suction are in satisfactory agreement with computed and experimental results of other investigators (Lai and So [24] and Hishida *et al.* [25]). The profile of $v\theta$, given by Lai and So [24], has been computed with a transport equation for the normal turbulent heat flux with no constant turbulent Prandtl number. It is shown that the peak value obtained by the eddy diffusivity model is lower than that computed by the more complete model of Lai and So [24].

The wall suction effects on the turbulent shear stress and heat flux are more pronounced for the highest suction rate (Figs 10 and 11). The absolute levels of both uv *and* $v\theta$ have been further reduced, when compared with those of Figs. 8 and 9 for $A = 0.46\%$, and all models produce the same level of decrease with the location of the maximum values predicted away from the pipe wall.

The distribution of $\overline{v\theta}$ in the near-wall region is presented in Fig. 12 for all suction rates examined. In addition, computed and experimental results of other investigators are included for $A = 0\%$, which indicate the good performance of the models in predicting the turbulent heat flux $v\theta$ for pipe flow with no suction. The dramatic decrease of the heat flux for the two suction rates is due to the normalization used, since the local values of the shear velocity $U*$ and friction temperature $\Theta*$ are increased due to suction.

The variation of c_f and Nu is shown in Fig. 13(a) and (b) for both suction rates. The increase in c_f and Nu is significant even for the smallest suction rate (0.46%) due to the increased values of τ_w and q_w (wall

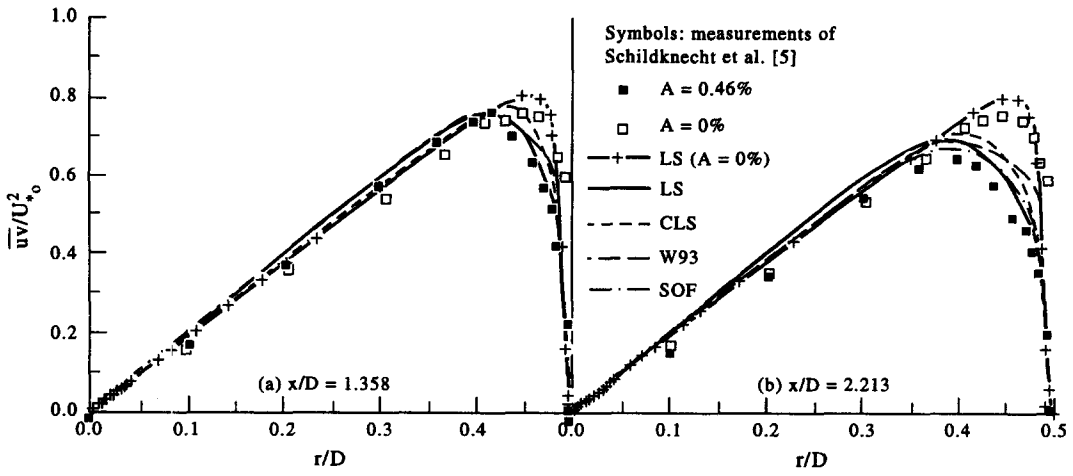

Fig. 8. Distribution of the turbulent shear stress for $A = 0.46\%$.

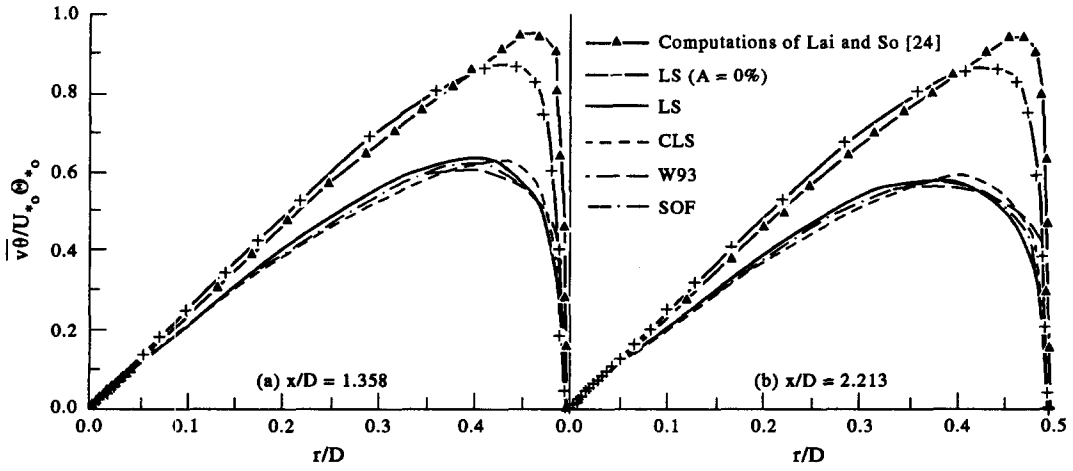

Fig. 9. Distribution of the normal turbulent heat flux for $A = 0.46\%$.

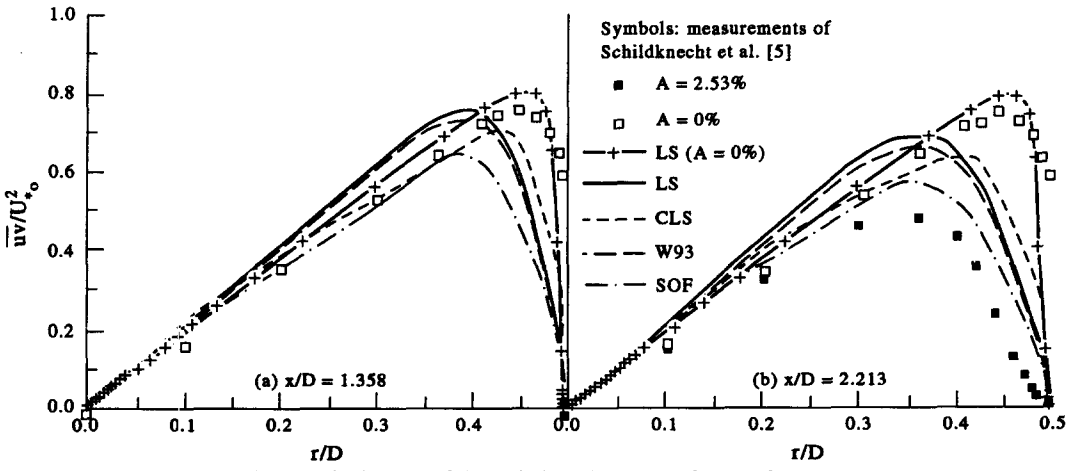

Fig. 10. Distribution of the turbulent shear stress for $A = 2.53\%$.

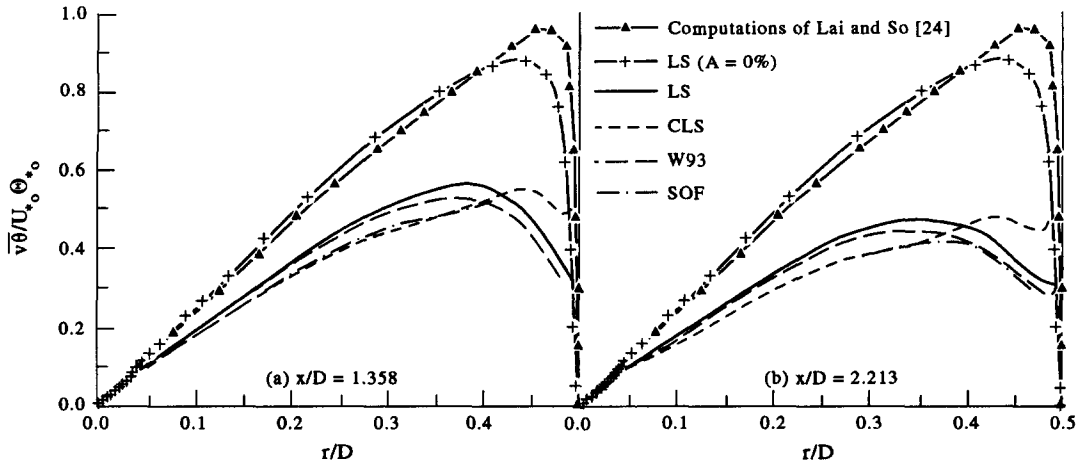

Fig. 11. Distribution of the normal turbulent heat flux for $A = 2.53\%$.

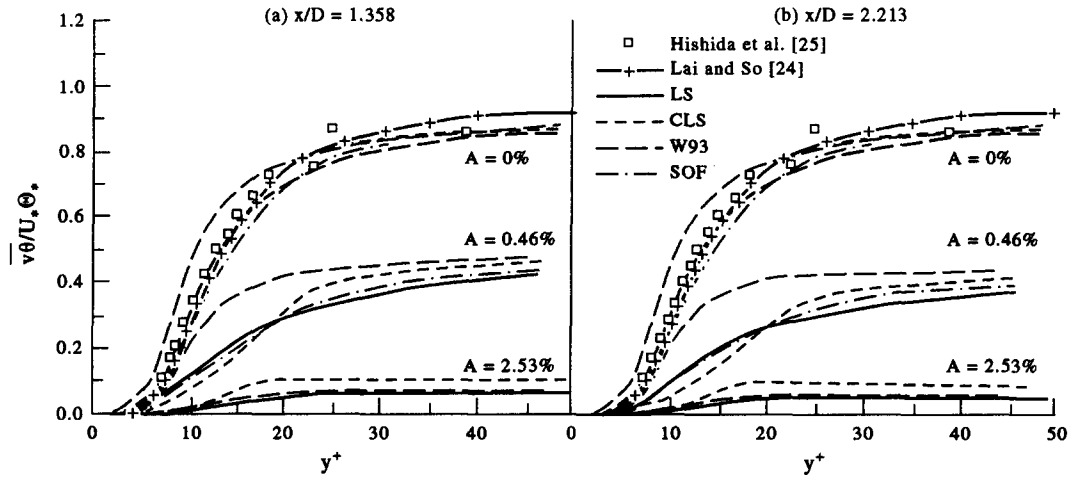

Fig. 12. Distribution of the normal turbulent heat flux in wall coordinates.

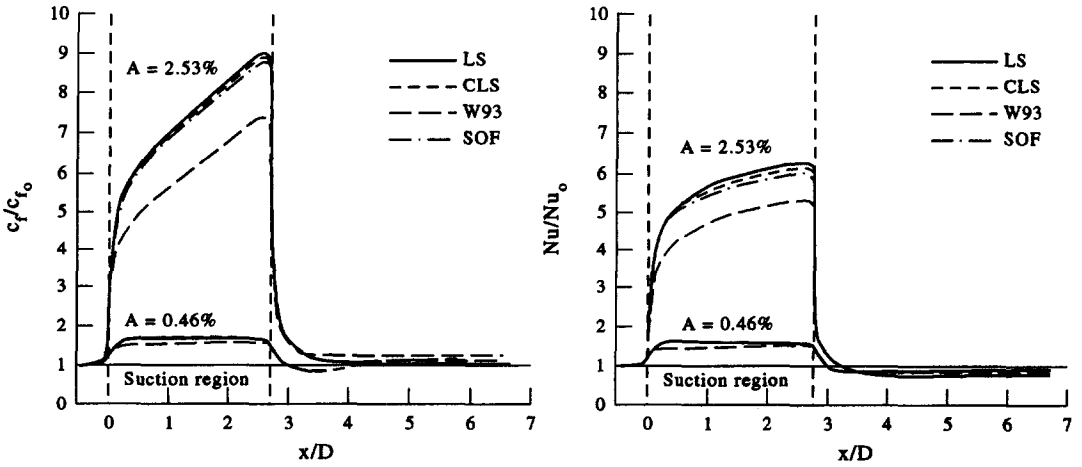

Fig. 13. Variation of c_f and Nu in the suction region.

heat flux) in the suction region. Such an increase is approximately 60% for c_f and 50% for the Nu. For $A = 2.53\%$ such an increase is much higher, and the excess in c_f and Nu resulting from suction is found to be 9 and 6 times, respectively, the values without suction. The W93 model produces a smaller increase than the other models.

6. CONCLUSIONS

The effects of wall suction on fluid flow and heat transfer rates in a pipe have been studied numerically for suction rates between 0.46 and 2.53%. Numerical results together with analytical solutions and experimental measurements indicate the following:

(a) Wall suction effects lead to more uniform mean velocity and temperature distributions with increased values in the near-wall region and reduced ones towards the centre line. Linear and non-linear EVMs used in the study are capable of predicting correctly the flow characteristics observed in the experiment. Computed and analytical velocity distributions are in satisfactory agreement with experimental measurements for the lowest suction rate ($A = 0.46\%$), indicating the validity of the boundary assumptions involved in the analytical solution. For the high suction rates ($A = 2.53\%$), these assumptions are not valid, and analytical results deviate from the computed and experimental ones, especially in the near-wall region.

(b) Wall suction effects are shown to modify the velocity and thermal law for the wall. The laminar sublayer is shown to decrease with increasing wall suction. Computed results and experimental measurements fall below the velocity and thermal law for the wall with no suction. For low suction rates, the von Karman constant has the same value as that with no suction, while, for high suction rates, the values of κ and κ_θ are no longer the same.

(c) Wall suction tends to decrease the levels of the turbulent shear stress $\overline{uv}$, indicating that inverse transition from turbulent to laminar flow would take place for a bigger suction length. The propagation of the suction effects in the interior of the flow is simulated by the turbulence models, with LS and SOF performing better.

(d) The normal turbulent heat flux $\overline{v\theta}$ is decreased significantly with increasing suction rate. Computed results for no suction are in satisfactory agreement with the computed and experimental results of other investigators.

(e) Increased c_f and Nu are calculated in the suction region for both suction rates. The increase in c_f (due to the increased boundary shear stress) is significant even for the smallest suction rate (up to 60%), while the increase is much higher for $A = 2.53\%$ (up to 900%). Similarly, the increase in Nu is approximately 50% for $A = 0.46\%$, while it is much higher (600%) for the highest suction rate examined (2.53%).

REFERENCES

1. Stevenson, T. N., A law of the wall for turbulent boundary layers with suction or injection. Aero. Report No. 166, Cranfield College of Aeronautics, 1963.
2. Verollet, E., Fulachier, L. and Dekeyser, I., Etude phenomenologique d'une couche limite turbulente avec aspiration et chauffage à la paroi. *International Journal of Heat and Mass Transfer*, 1977, **20,** 107–112.
3. Weissberg, H. L. and Berman, A. S., Velocity and pressure distribution in turbulent pipe flow with uniform suction. *Proceedings of the Heat Transfer Fluid Mechanics Institute*, University of California, Los Angeles, CA, 1955, pp. 1–30.
4. Aggarwal, J. K., Hollingsworth, M. A. and Mayhew, Y. R., Experimental friction factors for turbulent suction in a porous tube. *International Journal of Heat and Mass Transfer*, 1972, **15,** 1585–1595.
5. Schildknecht, M., Miller, J. A. and Meier, G. E. A., The influence of suction on the structure of turbulence in a fully developed pipe flow. *Journal of Fluid Mechanics*, 1979, **90,** 67–107.
6. Brosh, A. and Winograd, Y., Experimental study of turbulent flow in a tube with wall suction. *Journal of Heat Transfer, Transactions of ASME*, 1974, **94,** 338–342.
7. Elena, M., Etude des structures dynamiques et thermiques d'un ecoulement turbulent en conduite avec aspiration à la paroi. CEA-R-4843, Division de Chimie, Centre d'Etudes Nucleaires de Saclay, 1977.
8. Elena, M., Suction effects on turbulence statistics in a heated pipe flow. *Physics of Fluids*, 1984, **27,** 861–866.
9. Antonia, R. A., Fulachier, L., Krishnamoorthy, L. V., Benabid, T. and Anselmet, F., Influence of wall suction on the organized motion in a turbulent boundary layer. *Journal of Fluid Mechanics*, 1988, **190,** 217–240.
10. Kinney, R. B. and Sparrow, E. M., Turbulent flow, heat transfer and mass transfer in a tube with surface suction. *Journal of Heat Transfer, Transactions of ASME*, 1970, **92,** 117–125.
11. Merkine, L., Solan, A. and Winograd, Y., Turbulent flow in a tube with wall suction. *Journal of Heat Transfer, Transactions of ASME*, 1971, **93,** 242–244.
12. Medeiros, M. F., Pellegrini, C. C. and Silva-Freire, A. P., The turbulent boundary layer with addition of mass and heat. *Proceedings of the International Conference on Engineering Turbulence Modelling and Experiments*, Elsevier, Amsterdam, 1990, pp. 775–788.
13. Silva-Freire, A. P., An asymptotic solution for transpired incompressible turbulent boundary layers. *International Journal of Heat and Mass Transfer*, 1988, **31,** 1011–1021.
14. van Driest, E. R., On turbulent flow near a wall. *Journal of Aeronautical Science*, 1956, **23,** 1007–1010.
15. So, R. M. C. and Yoo, G. J., Low Reynolds number modelling of turbulent flows with and without wall transpiration. *AIAA Journal*, 1987, **25,** 1556–1564.
16. Launder, B. E. and Sharma, B. I., Application of the energy-dissipation model of turbulence to the calculation of flow near a spinning disk. *Letters in Heat and Mass Transfer*, 1974, **1,** 131–138.
17. Craft, T. J., Launder, B. E. and Suga, K., Extending the applicability of eddy viscosity models through the use of deformation invariants and non-linear elements. *Proceedings of the 5th International Symposium on Refined Flow Modelling and Turbulence Measurements*. Paris, 1993, pp. 125–132.

18. Suga, K., Personal communication, 1993.
19. Wilcox, D. C., Comparison of two-equation turbulence models for boundary layers with pressure gradient. *AIAA Journal*, 1993, **31**, 1414–1421.
20. Sofialidis, D., Strain-dependent, non-linear k–ω model of turbulence and its application. MSc. thesis, UMIST, Manchester, 1993.
21. Huang, P. G. and Leschziner, M. A., An introduction and guide to the computer code TEAM. TFD/83/09, Thermofluids Division, Department of Mechanical Engineering, UMIST, Manchester, 1983.
22. Leschziner, M. A., An introduction and guide to the computer code PASSABLE. TFD/82/11, Thermofluids Division, Department of Mechanical Engineering, UMIST, Manchester, 1982.
23. Johnk, R. E. and Hanratty, T. J., Temperature profiles for turbulent flow of air in a pipe—I. The fully developed heat transfer region. *Chemical Engineering Science*, **17**, 867–879.
24. Lai, Y. G. and So, R. M. C., Near-wall modelling of turbulent heat fluxes. *International Journal of Heat and Mass Transfer*, 1990, **33**, 1429–1440.
25. Hishida, M., Nagano, Y. and Tagawa, M., Transport processes of heat and momentum in the wall region of turbulent pipe flow. *Proceedings of the 8th International Heat Transfer Conference*, 1986, pp. 925–930.